Dynamics of confined colloid-polymer mixtures

Melissa Spannuth and Jacinta C. Conrad

Citation: AIP Conf. Proc. **1518**, 351 (2013); doi: 10.1063/1.4794596
View online: http://dx.doi.org/10.1063/1.4794596
View Table of Contents: http://proceedings.aip.org/dbt/dbt.jsp?KEY=APCPCS&Volume=1518&Issue=1
Published by the American Institute of Physics.

Dynamics of Confined Colloid-Polymer Mixtures

Melissa Spannuth and Jacinta C. Conrad

Department of Chemical and Biomolecular Engineering, University of Houston, Houston, TX 77006

Abstract. We investigate the effect of confinement on particle dynamics in mixtures of colloidal particles and non-adsorbing depletant polymers that serve as models for attractive suspensions. Holding the volume fraction of particles and the polymer concentration constant, the dynamics of the particles become increasingly slow as the suspensions are confined in thin wedge-shaped cells. Confocal micrographs of the confined samples suggest that clustering and solidification contribute to changes in the dynamics of mixtures in which particles interact via a strong attraction. The dynamics of non-aggregating particles that do not undergo a phase transition also become slower in confinement, suggesting that additional mechanisms must contribute to slow dynamics in confined colloid-polymer mixtures.

Keywords: colloids, depletion, confinement, gelation
PACS: 82.70.Dd, 47.57.J!, 64.75.Xc

1. INTRODUCTION

Confining colloidal suspensions in which the particles interact via a hard-sphere repulsion induces the formation of colloidal solids. For example, colloidal suspensions can crystallize when they are confined between parallel walls that are separated by less than ~ 20 particle diameters [1, 2], driven by the formation of layers of oscillating density at the walls [3]. If crystallization is suppressed, a fluid-like suspension can also solidify via a glass transition [4], driven by an increase in glassy structural order near the walls [5] or in wall-induced layering [6]. Both types of phase transition typically require that the particles be confined to a length of less than 10–20 times the particle diameter.

Solidification transitions induced by confinement influence the dynamics of the colloidal particles. Dynamics in both colloidal fluids [7, 8] and glasses [4, 9, 10] become increasingly slow in confinement, as measured by the mean-square displacement (MSD) $\left\langle \Delta x^2(\tau) \right\rangle = \left\langle (x(t+\tau)-x(t))^2 \right\rangle$ of the colloidal particles as a function of the lag time τ. For colloidal fluids, this slowing is most pronounced adjacent to the wall [7], which induces structural changes within the fluid [3] that lead to increased caging [8]. Counterintuitively, colloids in layers of higher density exhibit faster diffusive dynamics normal to the wall than those in layers of lower density [4, 11]. As the volume fraction of colloids ϕ is increased, the dynamics of particles in bulk liquid-like suspensions become arrested even at modest confinements, suggesting that confinement affects the length scale of dynamic heterogeneities [12, 13] that allow particles to rearrange and relax stress.

Effects of confinement on solidification and dynamics have been extensively investigated in suspensions of colloidal particles interacting *via* a hard-sphere repulsion. By contrast, how confinement affects the phase behavior and dynamics of suspensions of attractive colloidal particles is still poorly understood. These effects may be particularly important for microfabrication technologies such as spin-coating or rapid-prototyping, which shape particulate feedstocks into thin films [14] or rods [15]; for cell migration, which is driven by biological polymers such as actin [16] that are confined in thin lamellipodia [17]; or for the formation of surface-associated bacterial biofilms, which may be initiated by polymer-mediated attractions between micron-sized bacteria and surfaces [18, 19]. Understanding the effects of confinement on the structure and dynamics of particles in these complex systems would be facilitated by studies of simplified model systems, in which the strength and range of the attraction between particles can be precisely tuned.

Mixtures of nearly-hard-sphere micron-sized colloidal particles and non-adsorbing depletant polymers are particularly convenient model systems for attractive suspensions [20]. In such mixtures, the free volume of the polymer species is maximized when the excluded volume shells around the colloids overlap. The strength and range of the resultant entropic attraction are parameterized respectively by the concentration of polymer c_p and the ratio between the radius of gyration of the polymer and the colloid radius $\xi = r_g/a$. Precisely tuning c_p, ξ, and colloid volume fraction ϕ allows a variety of attractive colloidal phases to be formed, including fluids [21], crystals [22], glasses [23], and gels [24]. The first three phases have analogues in hard-sphere systems; gelation, however, requires a strong interparticle attraction. When the strength of the attraction is sufficiently large, colloid-polymer mixtures undergo spinodal decomposition into colloid-rich and colloid-poor phases [25]. The colloid-rich regions can solidify when the volume fraction of the

4th International Symposium on Slow Dynamics in Complex Systems
AIP Conf. Proc. 1518, 351-356 (2013); doi: 10.1063/1.4794596

particles approaches that of a colloidal glass, leading to the formation of space-spanning colloidal gels composed of clusters [26]. Colloidal gelation is therefore a consequence of equilibrium phase separation [27]. For phase-separating colloidal suspensions that do not solidify, confinement alters the phase behavior [28, 29, 30, 31, 32], for example by inducing capillary condensation [33].

Together, results from hard-sphere and from phase-separating attractive suspensions suggest that confinement may induce slow dynamics and solidification in colloid-polymer mixtures that can form gels. We have previously shown that confinement induces solidification in mixtures with a moderate-to-strong attraction by a different physical mechanism than that driving solidification in repulsive or hard-sphere suspensions. Specifically, we found that wall-induced layering is not responsible for gelation of colloid-polymer mixtures with a colloid volume fraction of $\phi = 0.15$; instead, confinement appears to increase the strength of the effective attraction between the colloidal particles [34].

In this paper, we study the effects of confinement on the dynamics of particles in colloid-polymer depletion mixtures. Using confocal microscopy and particle tracking, we measure the mean-squared displacements (MSDs) of particles in mixtures in which the particle volume fraction and polymer concentration are held constant, and show that confinement in a thin wedge chamber induces slowing of the particle dynamics. Comparison with micrographs of samples at different confinement thicknesses indicate that slowing of particle dynamics is driven in part by clustering of particles *en route* to gelation. In weakly attractive mixtures, however, we also observe confinement-induced slowing of dynamics, suggesting that additional mechanisms beyond clustering and solidification contribute to changes in dynamics of confined colloid-polymer mixtures.

2. EXPERIMENTAL METHODS

As a model system, we synthesized nearly-hard-sphere [35] poly(methylmethacrylate) colloidal particles of diameter $2a = 0.865\mu$m that were sterically stabilized by poly(12-hydroxysteric acid) polymers [36]. The particles were first dispersed in an index- and density-matching solvent mixture of cyclohexyl bromide (CXB) and decahydronaphthalene (DHN) at a ratio of 1:3 v/v. To minimize the effect of gravity on the phase behavior and structure of our samples, we added drops of CXB or DHN and confirmed that clusters and particles remain in suspensions after centrifugation at 800 g for 1.25 h. In these solvents the particles were charged [37], and so we added 1.5 mM of an organic salt, tetrabutyl(ammonium chloride), to all solvent mixtures to mitigate the slight electrostatic repulsion between particles. We confirmed that samples prepared with higher concentrations of salt (9 mM) exhibited the same behavior. To induce an effective depletion attraction between the colloids with controlled range and strength, we added non-adsorbing polystyrene of molecular weight $M_w = 295.8$ kDa with a radius of gyration $R_g = 15$ nm [38] and an overlap concentration $C_p^* = 3M_w/r\pi R_g^3 N_A \approx 35$ mg/mL. The range of the attraction $\xi = 0.035$ was approximately constant in these experiments. We fixed the volume fraction of colloids, $\phi \approx 0.15$, and varied the concentration of polymer from 0 to 23.6 mg/mL to increase the strength of the attraction between the particles. Table 1 lists the volume fraction and polymer concentration for each sample studied.

To rapidly access multiple confinements in a single experiment, we loaded samples into wedge-shaped glass chambers (Figure 1(a)). The opening angle of the chambers was $< 0.5°$, so that the walls were very nearly parallel. Measurements of the bulk viscosity of the suspensions as a function of the shear rate indicated that our samples behaved as either Newtonian ($C_p < 15$ mg/mL) or shear-thinning ($C_p > 15$ mg/mL) fluids at the typical shear rates applied during the loading of the chambers, suggesting that the samples are fully homogenized. Samples were allowed to rest for 30 min after loading in chambers and then imaged using confocal fluorescence microscopy [39] using a Visitech VT-Infinity confocal scanhead mounted on a Leica DMI4000 B microscope. We acquired three-dimensional image stacks at various positions along the wedge, corresponding to different thicknesses h ranging from $> 100\,\mu$m to $h < 6\,\mu$m. The accessible range of thicknesses normalized by the particle diameter was therefore $h/2a > 116$ to $h/2a < 7$. Finally, using standard algorithms [40] we located all particles in three dimensions and tracked their motion in two dimensions (in the x-y plane) at the midplane of the chamber (i.e. at $z = h/2$, where z is the direction along which the sample was confined). With these algorithms, we were able to locate the centroids of our particles to within 40 nm, as measured from the y-intercept of the MSD as a function of lag time. We confirmed that both ϕ and C_p remain constant along the wedge by respectively measuring particle density *via* Voronoi volumes and solvent viscosity *via* particle-tracking microrheology [41]. We also compared the structure and dynamics of samples in macroscopic chambers constructed from glass vials to those in the thickest region of the wedge to confirm that we measured bulk behavior in the wedge chambers. This experimental protocol therefore allowed us to sensitively assess the effects of confinement on the motility of particles at constant particle volume fraction and strength of attraction.

TABLE 1. Volume fraction and polymer concentration of samples.

Sample	**1**	**2**	**3**	**4**	**5**	**6**	**7**
ϕ	0.147	0.148	0.147	0.153	0.149	0.148	0.151
C_p [mg/mL]	0.0	10.4	12.9	15.5	17.7	20.7	23.6

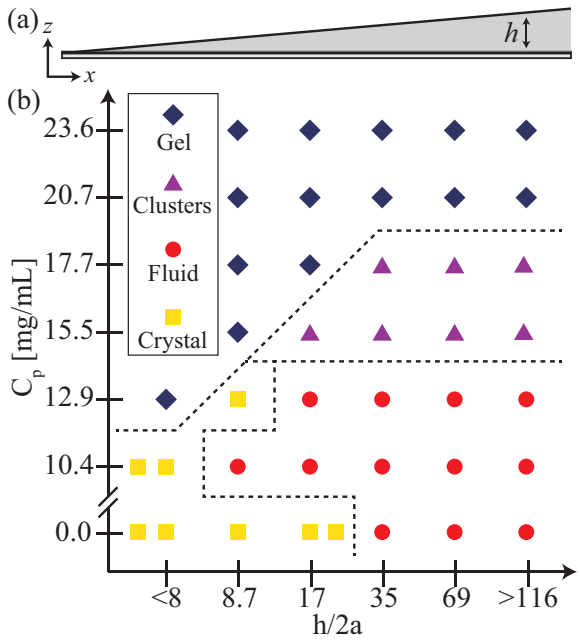

FIGURE 1. (Color online) (a) Schematic of the sample chambers used for confocal microscopy experiments, indicating the direction orthogonal to confinement (z) over which the confinement thickness h is measured. (b) Phase diagram for polymer concentration as a function of confinement, adapted from Reference [34]. Symbols indicate the phase: crystal (yellow □), fluid (red ○), fluid of clusters (purple), or gel (blue ◇). Dashed lines indicate guides to the eye.

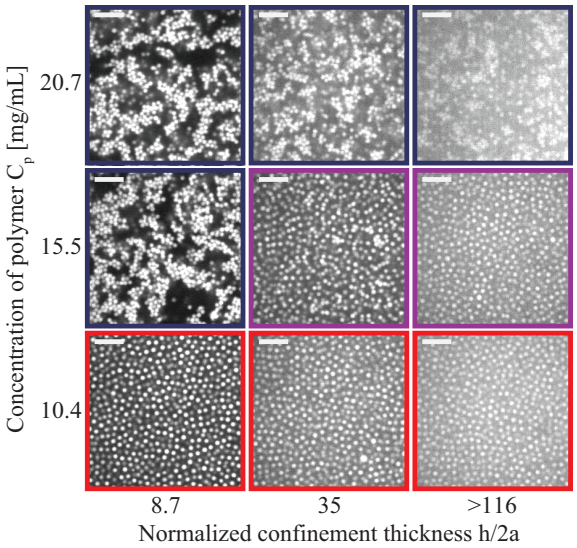

FIGURE 2. (Color online) Representative confocal micrographs of colloid-polymer samples at varying concentration of polymer C_p and confinement thickness h. Top row: $C_p = 20.7$ mg/mL (sample 6); middle row: $C_p = 15.5$ mg/mL (sample 4); bottom row: $C_p = 10.4$ mg/mL (sample 2). The color of the border around each micrograph indicates the phase as in Figure 1. Scale bars: 10 µm.

3. RESULTS

We have previously showed in Reference [34] that colloid-polymer mixtures solidify in confined geometries. Using both the structural information from particle pair correlation functions and the dynamic information from mean-squared displacements, we have identified four different colloidal phases: crystals, fluids, fluids of clusters, and gels. We find that the structure of fluids of clusters or gels with a moderate to strong interparticle attraction, parameterized by the concentration of polymer C_p, evolves as the suspensions are increasingly confined, as shown in Figure 2. For suspensions that solidify as the confinement is increased, changes in structure reflect the evolution towards the solid phase. For example, sample 4 ($C_p = 15.5$ mg/mL) when unconfined is a fluid of clusters and contains both dispersed particles and small clusters of particles, as shown in the middle row of micrographs in Figure 2. The size of clusters increases when this sample is confined to $h/2a = 35$; upon further confinement to $h/2a = 8.7$, the particles ultimately aggregate to form a space-spanning percolated gel. Changes in the structure of particles with increasing confinement are not restricted to samples undergoing a solidification transition. Sample 6 ($C_p = 20.7$ mg/mL) contains a percolated cluster at all confinement thicknesses $h/2a$ and hence is classified as a gel, as shown in the top row of images in Figure 2. As this sample is increasingly confined, both the fraction of particles in the percolating cluster and the thickness of the strands of the gel increase. By contrast, below a certain strength of attraction we observe no changes in the structure of disordered fluids, as shown for sample 2 ($C_p = 10.4$ mg/mL) in the bottom row of Figure 2. Only when the sample is confined to very small thicknesses ($h/2a < 8$) does the sample form an ordered crystal.

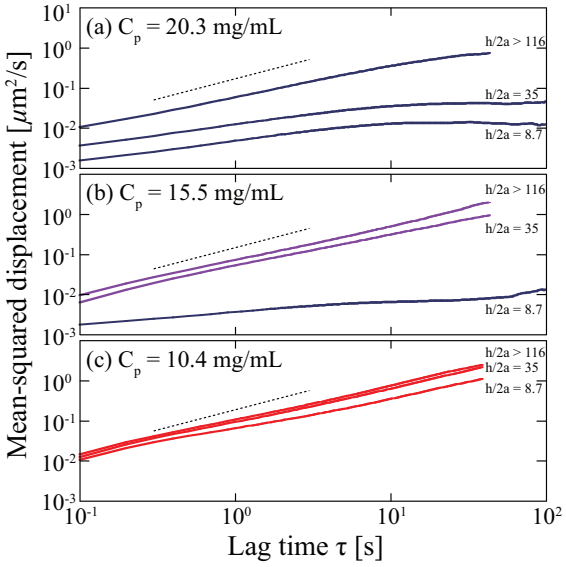

FIGURE 3. (Color online) Mean-squared displacement as a function of lag time τ. (a) Sample 6 ($C_p = 20.3$ mg/mL) at $h/2a > 116$ and $h/2a = 35$ and 8.7 (top to bottom, all gels). (b) Sample 4 ($C_p = 15.5$ mg/mL) at $h/2a > 116$ and $h/2a = 35$ (fluids of clusters) and $h/2a = 8.7$ (gel). (c) Sample 2 ($C_p = 10.4$ mg/mL) at $h/2a > 116$ and $h/2a = 35$ and 8.7 (top to bottom, all fluids). Dashed lines indicate slope of 1. Colors indicate the phase as in Figure 1.

We quantify changes in dynamics with increasing confinement *via* the mean-squared displacement (MSD) as a function of lag time τ. For all samples investigated, confinement induces slowing in the particle dynamics, as indicated by the decreases in the MSD with increasing confinement in Figure 3. Moreover, slowing occurs regardless of structural evolution. For example, sample 4 (shown in Figure 3(b)) undergoes a transition from a fluid of disconnected clusters (at $h/2a = 35$) to a percolating gel (at $h/2a = 8.7$) as it is increasingly confined; concomitantly, the MSD decreases by over an order of magnitude. To demonstrate that phase transitions are not solely responsible for changes in particle dynamics in confinement, we calculate the MSD for sample 6, which is a gel at all values of $h/2a$. The MSD of sample 6 similarly decreases by about an order of magnitude as the sample is confined from bulk ($h/2a > 116$) to $h/2a = 8.7$. To demonstrate that structural changes are not required for confinement-induced slowing of dynamics, we calculate the MSD for sample 2, which is a fluid at all confinements $h/2a > 8$. The structure of sample 2 (as measured by the fraction of particles in clusters) does not evolve over this range of confinements; nonetheless, the MSD decreases as the sample is confined from $h/2a > 116$ to $h/2a = 8.7$.

To gain insight into the physical processes that drive slowing of particle dynamics in confined colloid-polymer mixtures, we first examine the MSD at a fixed lag time $\tau = 10$ s, corresponding to approximately 10 times the self-diffusion time of a single particle (Figure 4). The magnitude of the MSD at $\tau = 10$ s for sample 4, which undergoes a gelation transition between $h/2a = 17$ and $h/2a = 8.7$, decreases by over an order of magnitude. In contrast to results obtained for hard-sphere colloidal supercooled fluids [4, 6], the MSD at fixed lag time does not always decrease sharply at the transition from a fluid-like phase to a solid-like phase. Indeed, both crystallization and gelation transitions can occur without a dramatic change in the magnitude of the MSD. For example, the crystallization transition in sample 2 and the gelation transitions in samples 3 and 5 are accompanied by only modest dynamical slowing. In addition, changes in the dynamics occur over a surprisingly large range of confinement thicknesses $h/2a$. This effect is most pronounced for gel samples 6 and 7, but even sample 5 exhibits a notable slowing of dynamics at large $h/2a$ far from solidification. Together, these results suggest that solidification transitions and the accompanying changes in structure do not completely account for the slowing of dynamics of particles in confined colloid-polymer mixtures.

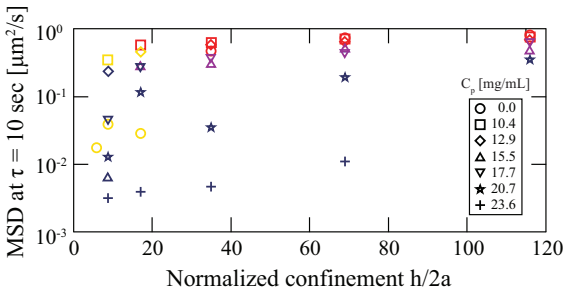

FIGURE 4. (Color online) Mean-squared displacement at fixed lag time $\tau = 10$ s as a function of normalized confinement thickness $h/2a$ for samples 1 (○), 2 (□), 3 (◇), 4 (△), 5 (▽), 6 (★), and 7 (+). Colors indicate the phase as in Figure 1.

We investigate the effect of the lag time τ on the dynamics *via* the self-part of the van Hove correlation function, $G_s(x,\tau) = (1/N)\sigma_{i=1}^{N}\delta\,[x + x_i(0) - x_i(\tau)]$ [42], which represents the probability of a displacement x over a time interval τ. $G_s(x,\tau)$ measured for fluids and for gels exhibit distinct shapes in unconfined samples, as shown in Figure 5(a) for bulk or near-bulk samples. For a fluid sample that contains no polymer and in which the particles thus interact *via* an electrostatic repulsion (sample 1), $G_s(x,\tau)$ can be well-fit by a single Gaussian function, $G_s(x,\tau) = a_1 \exp(-x^2/\sigma_1^2)$, as shown by the long-dashed line in Figure 5(a). The characteristic displacement of particles estimated from the width of this distribution, $\sigma_1 \approx 1.2$ μm, is in good agreement with the ex-

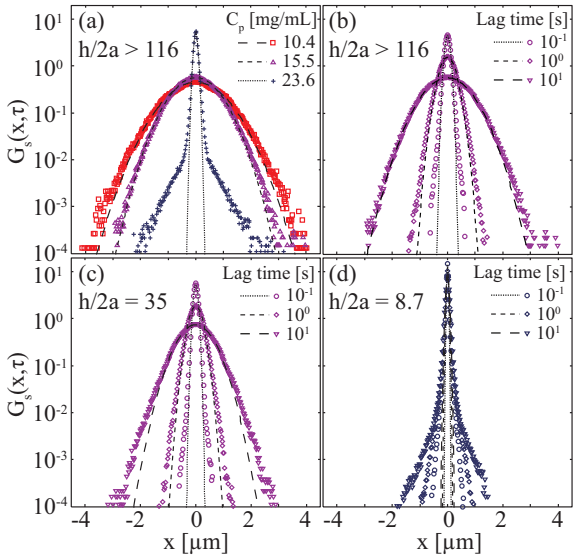

FIGURE 5. (Color online) (a) Self-part of the van Hove correlation $G_s(x,\tau)$ at $\tau = 10$ s for bulk ($h/2a > 116$) samples 2 (fluid,) and 4 (fluid of clusters,) and for sample 7 at confinement thickness $h/2a = 67$ (gel, +). Lines indicate fits to single Gaussian functions. (b)–(d) $G_s(x,\tau)$ for sample 4 at confinement thickness (b) $h/2a > 116$ (fluid of clusters), (c) $h/2a = 35$ (fluid of clusters), and (d) $h/2a = 8.7$ (gel). In (b)–(d), $\tau = 0.1$ s (○), 1 s (◇), and 10 s (). Lines indicate fits to single-Gaussian distributions. Colors indicate the phase as in Figure 1.

pected displacement for a freely-diffusing particle over a time scale τ, $\sqrt{D_0 t} \approx 1.3$ μm, where $D_0 = k_B T/6\pi\eta_0 a$ is the diffusion coefficient calculated at room temperature using the background solvent viscosity $\eta_0 \approx 2.7$ mPa-s. As the strength of the interparticle attraction is increased (e.g. sample 4, in which $C_p = 15.5$ mg/mL), $G_s(x,\tau)$ can still be described by a single Gaussian function. The characteristic displacement estimated from σ_1, however, is smaller than that of the repulsive sample, reflecting both the increase in background solvent viscosity due to the polymer and the formation of clusters of particles (visible in Figure 2). Finally, when the strength of the attraction between particles is further increased (e.g. sample 7, in which $C_p = 23.6$ mg/mL), $G_s(x,\tau)$ is sharply peaked around $x = 0$, consistent with locally caged motion, and exhibits broad exponential tails, consistent with sporadic large jumps [43, 44]. We conclude that in near-bulk samples, the shape of $G_s(x,\tau)$ reflects the phase behavior of the underlying sample.

We probe the effect of confinement on dynamics in colloid-polymer mixtures by measuring $G_s(x,\tau)$ at different confinement thicknesses $h/2a$ and at different lag times τ for sample 4, which undergoes a fluid-to-gel transition with increasing confinement. In a bulk sample (i.e. for $h/2a > 116$), $G_s(x,\tau)$ for $\tau = 10$ s is well fit by a single Gaussian function at lag times τ ranging from 0.1 s to 10 s, as shown in Figure 5(b). When this sample is confined to a height $h/2a = 35$, the widths of the Gaussian fits are slightly smaller than those obtained in bulk (Figure 5(c)). As the concentration of polymer and hence the viscosity of the background solution does not change along the wedge and the phase of the sample is similar, this finding confirms that confinement induces changes in the dynamics of the particles. The quality of the single Gaussian fit decreases at all values of τ as compared to that of the unconfined sample, consistent with our earlier finding that the fraction of particles in clusters increases in confinement [34]. Finally, when sample 4 is confined below $h/2a = 8.7$, the particles form a percolated space-spanning network and $G_s(x,\tau)$ exhibits the characteristic shape for a gel. The characteristic width σ_1 of the single-Gaussian fit to the sharp peak in $G_s(x,\tau)$ increases only slightly as τ is increased, suggesting that particles are trapped in local cages over all measured lag times. The van Hove correlation functions for sample 4 measured at varying τ and $h/2a$ suggest that confinement-induced slow dynamics in colloid-polymer mixtures result in part from clustering and gelation induced at small $h/2a$. We have also examined $G_s(x,\tau)$ for varying τ and $h/2a$ for sample 2, which is a disordered fluid for $h/2a > 8$. The systematic decrease in the width of $G_s(x,\tau)$ for this sample, in which the particles do not aggregate into clusters, suggests that additional mechanisms beyond clustering and solidification must contribute to changes in particle dynamics in confinement.

CONCLUSIONS

Confining mixtures of colloids and non-adsorbing particles between two nearly parallel walls induces slowed dynamics of the particles. By examining dynamical measurements of the mean-squared displacement and the self part of the van Hove correlation function, we conclude that confinement-induced crystallization [45] or gelation [46] fluid-to-solid transitions, in which particles become increasingly localized [46], contribute in part to the decrease in particle MSD observed for colloid-polymer mixtures in which the particles exhibit a strong effective attraction. Mixtures in which the structure of particles does not change in confinement also exhibit changes in dynamics, however, indicating that changes in structure and phase do not completely account for the confinement-induced changes in dynamics. Further experiments to determine the relative importance of confinement and phase transitions on the dynamics of particles in confined colloid-polymer mixtures may yield new understanding into the mechanisms of confined solidification in attractive suspensions.

ACKNOWLEDGMENTS

This work was supported by the American Chemical Society Petroleum Research Fund (52537-DNI7) and by seed grants from the Texas Center for Superconductivity and the University of Houston Grants to Enhance and Aid Research. We thank R. Krishnamoorti and F. Babaye Khorasani for helpful discussions.

REFERENCES

1. P. Pieranski, L. Strzelecki, and B. Pansu, *Phys. Rev. Lett.* **50**, 900–903 (1983).
2. D. H. V. Winkle, and C. A. Murray, *Phys. Rev. A* **34**, 562–573 (1986).
3. D. H. Van Winkle, and C. A. Murray, *J. Chem. Phys.* **89**, 3885–3891 (1988).
4. C. R. Nugent, K. V. Edmond, H. N. Patel, and E. R. Weeks, *Phys. Rev. Lett.* **99**, 025702 (2007).
5. K. Watanabe, T. Kawasaki, and H. Tanaka, *Nat. Mater.* **10**, 512–520 (2011).
6. K. V. Edmond, C. R. Nugent, and E. R. Weeks, *Phys. Rev. E* **85**, 041401 (2012).
7. H. B. Eral, D. Van Den Ende, F. Mugele, and M. H. G. Duits, *Phys. Rev. E* **80**, 061403 (2009).
8. H. B. Eral, F. Mugele, and M. H. G. Duits, *Langmuir* **27**, 12297–12303 (2011).
9. V. N. Michailidou, G. Petekidis, J. W. Swan, and J. F. Brady, *Phys. Rev. Lett.* **102**, 068302 (2009).
10. K. V. Edmond, C. R. Nugent, and E. R. Weeks, *Eur. Phys. J. Special Topics* **189**, 83–93 (2010).
11. J. Mittal, T. M. Truskett, J. R. Errington, and G. Hummer, *Phys. Rev. Lett.* **100**, 145901 (2008).
12. P. Sarangapani, A. B. Schofield, and Y. Zhu, *Phys. Rev. E* **83**, 030402 (2011).
13. P. Sarangapani, A. B. Schofield, and Y. Zhu, *Soft Matter* **8**, 814–818 (2012).
14. L. T. Shereda, R. G. Larson, and M. J. Solomon, *Phys. Rev. Lett.* **101**, 038301 (2008).
15. J. A. Lewis, *Adv. Funct. Mater.* **16**, 2193 (2006).
16. M. Soares e Silva, J. Alvarado, J. Nguyen, N. Georgoulia, B. M. Mulder, and G. H. Koenderink, *Soft Matter* **7**, 10631–10641 (2011).
17. J. Stricker, T. Falzone, and M. L. Gardel, *J. Biomech.* **43**, 9–14 (2010).
18. J. Schwarz-Linek, A. Winkler, L. G. Wilson, N. T. Pham, C. E. French, T. Schilling, and W. C. K. Poon, *Soft Matter* **6**, 4540–4549 (2010).
19. J. Schwarz-Linek, G. Dorken, A. Winkler, L. G. Wilson, N. T. Pham, C. E. French, T. Schilling, and W. C. K. Poon, *EPL* **89**, 68003 (2010).
20. S. M. Ilett, A. Orrock, W. C. K. Poon, and P. N. Pusey, *Phys. Rev. E* **51**, 1344–1352 (1995).
21. D. G. A. L. Aarts, R. Tuinier, and H. N. W. Lekkerkerker, *J. Phys.: Condens. Matter* **14**, 7551–7561 (2002).
22. D. M. Herlach, I. Klassen, P. Wette, and D. Holland-Moritz, *J. Phys.: Condens. Matter* **22**, 153101 (2010).
23. K. N. Pham, A. M. Puertas, J. Bergenholtz, S. U. Egelhaaf, A. Moussaid, P. N. Pusey, A. B. Schofield, M. E. Cates, M. Fuchs, and W. C. K. Poon, *Science* **296**, 104–106 (2002).
24. E. Zaccarelli, *J. Phys.: Condens. Matter* **19**, 323101 (2007).
25. H. N. W. Lekkerkerker, W. C. K. Poon, P. N. Pusey, A. Stroobants, and P. B. Warren, *Europhys. Lett.* **20**, 559–564 (1992).
26. N. A. M. Verhaegh, D. Asnaghi, H. N. W. Lekkerkerker, M. Giglio, and L. Cipelletti, *Physica A* **242**, 104–118 (1997).
27. P. J. Lu, E. Zaccarelli, F. Ciulla, A. B. Schofield, F. Sciortino, and D. A. Weitz, *Nature* **453**, 499–504 (2008).
28. M. Schmidt, A. Fortini, and M. Dijkstra, *J. Phys.: Condens. Matter* **16**, S4159–S4168 (2004).
29. R. L. C. Vink, A. De Virgiliis, J. Horbach, and K. Binder, *Phys. Rev. E* **74**, 031601 (2006).
30. A. De Virgiliis, R. L. C. Vink, J. R. Horbach, and K. Binder, *Phys. Rev. E* **78**, 041604 (2008).
31. K. Binder, J. R. Horbach, R. L. C. Vink, and A. De Virgiliis, *Soft Matter* **4**, 1555–1568 (2008).
32. D. Burch, and M. Z. Bazant, *Nano Lett.* **9**, 3795–3800 (2009).
33. D. G. A. L. Aarts, and H. N. W. Lekkerkerker, *J. Phys.: Condens. Matter* **16**, S4231–S4242 (2004).
34. M. Spannuth, and J. C. Conrad, *Phys. Rev. Lett.* **109**, 028301 (2012).
35. C. P. Royall, W. C. K. Poon, and E. R. Weeks, *Soft Matter*, doi:10.1039/c2sm26245b (2013).
36. L. Antl, J. W. Goodwin, R. D. Hill, R. H. Ottewill, S. M. Owens, S. Papworth, and J. A. Waters, *Colloid Surf.* **17**, 67–78 (1986).
37. A. Yethiraj, and A. van Blaaderen, *Nature* **421**, 513–517 (2003).
38. G. C. Berry, *J. Chem. Phys.* **44**, 4550–4564 (1966).
39. A. D. Dinsmore, E. R. Weeks, V. Prasad, A. C. Levitt, and D. A. Weitz, *Appl. Opt.* **40**, 4152–4159 (2001).
40. J. C. Crocker, and D. G. Grier, *J. Colloid Interface Sci.* **179**, 298–310 (1996).
41. T. G. Mason, and D. A. Weitz, *Phys. Rev. Lett.* **74**, 1250–1253 (1995).
42. A. Rahman, *Phys. Rev.* **136**, A405–A411 (1964).
43. Y. Gao, and M. L. Kilfoil, *Phys. Rev. Lett.* **99**, 078301 (2007).
44. Y. Gao, and M. L. Kilfoil, *Phys. Rev. E* **79**, 051406 (2009).
45. A. M. Alsayed, M. F. Islam, J. Zhang, P. J. Collings, and A. G. Yodh, *Science* **309**, 1207–1210 (2005).
46. C. J. Dibble, M. Kogan, and M. J. Solomon, *Phys. Rev. E* **74**, 041403 (2006).